

Optimal photon-pair single mode coupling in narrow-band spontaneous parametric down-conversion with arbitrary pump profile

Jean-Loup Smirr, Matthieu Deconinck, Robert Frey, Imad Agha, Eleni Diamanti, and Isabelle Zaquine*

Institut TELECOM/Telecom ParisTech – CNRS/LTCI

46 rue Barrault 75013 PARIS, France

(Dated: 2011)

A theoretical study of the performance of single-mode coupled spontaneous parametric down-conversion sources is proposed, which only requires very few assumptions of practical interest : narrow-bandwidth and quasi-degenerate collinear generation. Other assumptions like pump beam spatial and temporal envelopes, target single-mode profile and size, and non-linear susceptibility distribution, are only taken into account in the final step of the computation, thus making the theory general and flexible. Figures of merit for performance include absolute collected brightness, pair collection efficiency and heralding ratio. The optimization of these values is investigated through functions that only depend on dimensionless parameters, allowing for deducing from the results the best experimental configuration for a whole range of design choices (e.g. crystal length, pump power). A particular application of the theory is validated by an experimental optimization obtained under compatible assumptions. A comparison with other works and proposals for numerically implementing the theory in its most generality are also provided.

I. INTRODUCTION

Sources of entangled photons have applications ranging from fundamental tests of quantum mechanics [1, 2] to quantum information and communications [3, 4]. Entanglement based quantum key distribution protocols have been reported [5] as an alternative to those based on single photon sources and quantum repeaters have also been shown to require entanglement as a primary resource [6, 7].

Spontaneous parametric down-conversion (SPDC) remains the simplest way to generate entangled photons, enabling telecom wavelength generation which cannot be easily achieved using atomic cascades. A large choice of configurations is available according to the emission geometry (collinear [8] or not [9, 10]), the phase matching type (I [11] or II [9]) and the signal and idler frequencies (degenerate [12] or not [13]). The non-collinear emission geometry has some advantages, providing direct separation of signal and idler photons but collinear emission in periodically poled crystals recently became increasingly popular [14–16], because of the high brightness obtained with longer crystals and higher nonlinear susceptibilities.

Filtering is one of the most important aspects of photon pair engineering. Spatial filtering and more specifically coupling the photon pairs to a single spatial mode, like an optical fiber, is the first requirement for long-distance communications. The coupling efficiency is then a key parameter, knowing that losses directly limit the maximum possible visibility of the source [17, 18]. Narrow-band spectral filtering can be necessary to ensure spectral indistinguishability but also to obtain efficient coupling to a quantum memory [19–22]. It is also beneficial for long-distance communications of polarization states as it reduces polarization mode dispersion.

Since the pioneering works of SPDC concerning the quantum fluctuation and noise in parametric processes [23] and those dealing with probability of coincidences in the emission of signal and idler photons [24–26] an important theoretical effort has been developed in order to optimize various kind of sources [27, 28], some of them dedicated to strongly focused beams [29].

After studies of the collection of SPDC through apertures [30, 31], numerous authors have reported studies of the coupling of SPDC into a single spatial mode like that of a fiber [32–38], with various assumptions and experimental methods of validation.

The optimal focusing of a continuous wave monochromatic pump has been investigated [35] in order to calculate the maximum coupling efficiency of photon pairs into single-mode fibers but the pump diffraction was neglected and the phase mismatch was not taken into account in the optimization process. The same approximations have been used in [36] to calculate the absolute emission rates of SPDC into single modes, where the crystal is moreover assumed to be thin. The absolute brightness is also calculated in [37] but with a continuous wave pump, emphasizing the parallel between SPDC and the classical treatment used for second harmonic generation. Very recently, R. S. Bennink studied the case of Gaussian beam profiles, directly writing the nonlinear interaction hamiltonien with a gaussian beam profile for both the pump and the SPDC generated photon pairs [38]. In this case, neither the absolute brightness of the source nor the absolute collection efficiency of an optical fiber can be evaluated. Moreover, no spectral filtering is taken into account.

To our knowledge, a comprehensive study of narrow-band SPDC pumped by a diffracting beam of arbitrary pulse envelope and duration (from short pulses to continuous-wave lasers) and arbitrary transverse profile, covering a full range of focusing (from tight focusing to parallel beams) and arbitrary filter shapes, has not been

* isabelle.zaquine@telecom-paristech.fr

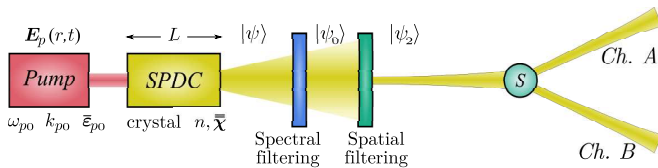


FIG. 1. General configuration considered in the theoretical framework: a nonlinear crystal is pumped by a beam of arbitrary temporal and spatial profiles. The photon pairs produced through SPDC are spectrally filtered and coupled to a single spatial mode, before being split towards channels A and B.

addressed. Such a generalization can, however, be useful in view of optimizing future SPDC sources that might require specific spectral and spatial characteristics to interface with particular quantum information systems.

In this paper, we propose a theoretical framework that is general enough to allow the investigation of these characteristics and their effects on the source performance (e.g. brightness, coupling efficiency) under assumptions suited to the desirable characteristics mentioned above: narrow-bandwidth for quantum information applications and colinear emission in long crystals with a given non-linear susceptibility distribution. Using a dedicated source, we also experimentally validate the theoretical predictions for particular assumptions.

Section II describes the general formalism of the addressed problem and derives the wave-function of the created photon pairs, taking into account spatial and spectral filtering. We also define various figures of merit that are useful to characterize a source performance. The numerical application of this general theoretical approach to the case of a narrow-band fibered source pumped by a Gaussian beam is developed in section III. The experimental setup is described in section IV and the measured performances are compared with the theoretical predictions. A comparison of our results with other works, as well as guidelines for generalizing the numerical calculations are proposed in section V.

II. THEORETICAL FRAMEWORK

A. The down-converted two-photon state

The general configuration considered hereafter is depicted in Figure 1. The non-linear interaction takes place in a crystal with a second-order susceptibility $\overline{\chi}^{(2)}(\mathbf{r})$, pumped by a classical field of positive-frequency complex amplitude $\mathbf{E}_p^{(+)}$. The spontaneous parametric down-conversion process is described by a time-dependent Hamiltonian $\hat{\mathcal{H}}(t)$. The signal and idler fields, $\hat{\mathbf{E}}_s^{(+)}$ and $\hat{\mathbf{E}}_i^{(+)}$, have the following plane-wave decomposition in the

quantization volume \mathcal{V} :

$$\hat{\mathbf{E}}_{s,i}^{(+)}(\mathbf{r}, t) = \sum_{\ell_{s,i}} \vec{\epsilon}_{\ell_{s,i}} \hat{a}_{\ell_{s,i}} A(\ell_{s,i}) e^{i(\mathbf{k}_{\ell_{s,i}} \cdot \mathbf{r} - \omega_{\ell_{s,i}} t)} \quad (1)$$

where the field amplitude $A(\ell)$ for the mode ℓ associated with annihilation operator \hat{a}_{ℓ} is

$$A(\ell) = i \sqrt{\frac{\hbar \omega_{\ell}}{2\epsilon_0 \mathcal{V} n^2(\mathbf{k}_{\ell})}}, \quad (2)$$

Frequency and polarization are respectively denoted by ω_{ℓ} and $\vec{\epsilon}_{\ell}$, wavevectors in the crystal by \mathbf{k}_{ℓ} . A notation \mathbf{k}'_{ℓ} will be used when the wavevector is evaluated in another medium.

In the interaction picture, the Hamiltonian is given by [39, 40]

$$\hat{\mathcal{H}}(t) = \epsilon_0 \int d^3\mathbf{r} \mathbf{E}_p^{(+)}(\mathbf{r}, t) \overline{\chi}^{(2)}(\mathbf{r}) \hat{\mathbf{E}}_s^{(-)}(\mathbf{r}, t) \hat{\mathbf{E}}_i^{(-)}(\mathbf{r}, t) + H.c. \quad (3)$$

where $\hat{\mathbf{E}}^{(-)}$ is the Hermitian conjugate (*H.c.*) of $\hat{\mathbf{E}}^{(+)}$.

The pump field is assumed to be a linearly $\vec{\epsilon}_x$ -polarized classical paraxial beam propagating along the z axis with L^2 -normalized temporal and spatial envelopes T_p and S_p .

Using transverse coordinates $\boldsymbol{\rho} = \begin{pmatrix} x \\ y \end{pmatrix}$ so that $\mathbf{r} = \begin{pmatrix} \boldsymbol{\rho} \\ z \end{pmatrix}$

$$\mathbf{E}_p^{(+)}(\boldsymbol{\rho}, z, t) = \vec{\epsilon}_x C_p T_p \left(t - \frac{z}{v_p} \right) S_p(\boldsymbol{\rho}, z) e^{i(k_{p0} z - \omega_{p0} t)}. \quad (4)$$

Here k_{p0} is the pump wavevector modulus at its central frequency ω_{p0} and v_p is the group velocity in the crystal. We neglect its spectral dispersion, therefore $v_p = c/n_p$ where n_p is the refractive index in the crystal at ω_{p0} . The constant $C_p = \sqrt{\mathcal{E}_p / (2\epsilon_0 n_p^2 v_p)}$ depends on the pump pulse energy \mathcal{E}_p .

When the down-conversion efficiency is small, the generated two-photon state is the first-order approximate solution to the Schrödinger equation. Discarding the zeroth-order term

$$|\psi(t)\rangle = \frac{1}{i\hbar} \int_{-\infty}^t dt' \hat{\mathcal{H}}(t') |0\rangle. \quad (5)$$

Let us separate the spatial dependence $R(\mathbf{r})$ of the non-linear susceptibility

$$\vec{\epsilon}_x \overline{\chi}^{(2)}(\mathbf{r}) \vec{\epsilon}_{\ell_s} \vec{\epsilon}_{\ell_i} = \chi(\ell_s, \ell_i) \cdot R(\mathbf{r}). \quad (6)$$

After the pump has propagated through the whole crystal length, ($t \rightarrow \infty$), the state is time-independent in the interaction picture. Identifying the integral in Eq. (5) as a Fourier transform of $E_p^{(+)} = \mathbf{E}_p^{(+)} \cdot \vec{\epsilon}_x$ with respect to its temporal variable and according to the Fourier transform conventions of Appendix A, the state is given by

$$|\psi\rangle = \frac{\epsilon_0}{i\hbar} \sum_{\ell_s, \ell_i} \chi(\ell_s, \ell_i) A(\ell_s) A(\ell_i) \int d^3\mathbf{r} e^{-i(\mathbf{k}_{\ell_s} + \mathbf{k}_{\ell_i}) \cdot \mathbf{r}} \times R(\mathbf{r}) \check{E}_p^{(+)}(\mathbf{r}, \omega_{\ell_s} + \omega_{\ell_i}) \hat{a}_{\ell_s}^{\dagger} \hat{a}_{\ell_i}^{\dagger} |0\rangle. \quad (7)$$

This equation can be understood as the sum of the contributions of local interactions to the delocalized down-converted two-photon state $|\psi\rangle$. The integral has the form of a spatial Fourier transform, which leads to

$$|\psi\rangle = \sum_{\ell_s, \ell_i} \gamma_0(\ell_s, \ell_i) \hat{a}_{\ell_s}^\dagger \hat{a}_{\ell_i}^\dagger |0\rangle, \quad (8)$$

where

$$\gamma_0(\ell_s, \ell_i) = \frac{\epsilon_0}{i\hbar} \chi(\ell_s, \ell_i) A(\ell_s) A(\ell_i) \times \check{R} * \check{E}_p^{(+)}(\mathbf{k}_{\ell_s} + \mathbf{k}_{\ell_i}, \omega_{\ell_s} + \omega_{\ell_i}), \quad (9)$$

\check{R} being the Fourier transform of R . Using the fact that, for a diffracting beam in the paraxial approximation, the Fourier transform of the transverse spatial envelope has the following z dependence

$$\check{S}_p(\boldsymbol{\kappa}, z) = \check{S}_p(\boldsymbol{\kappa}, 0) e^{-i\frac{|\boldsymbol{\kappa}|^2}{2k_{p0}}z}, \quad (10)$$

where $\boldsymbol{\kappa}$ is the transverse wavevector, we have, according to the Fourier transform conventions of Appendix A :

$$\check{E}_p^{(+)}(\boldsymbol{\kappa}, k_z, \omega) = C_p \check{T}_p(\omega - \omega_{p0}) \check{S}_p(\boldsymbol{\kappa}, 0) \times 2\pi\delta\left(k_z - k_{p0} - \frac{\omega - \omega_{p0}}{v_p} + \frac{|\boldsymbol{\kappa}|^2}{2k_{p0}}\right). \quad (11)$$

We consider a crystal of length L centered on $z = 0$ whose transverse dimensions are large compared to the pump beam profile. If its nonlinear susceptibility distribution is transversally invariant, it can be expressed as a one-dimensional Fourier series

$$R(z) = \text{rect}(z/L) \times \sum_m R_m e^{-i2\pi m \frac{z}{L}}, \quad (12)$$

where $\text{rect}(z)$ is the rectangular function, with $\text{rect}(0) = 1$. In the reciprocal space,

$$\check{R}(k_z) = \sum_m R_m \text{sinc}(k_z + 2\pi m/L). \quad (13)$$

Then $\gamma_0(\ell_s, \ell_i) = \sum_m \gamma_{0m}(\ell_s, \ell_i)$ with

$$\begin{aligned} \gamma_{0m}(\ell_s, \ell_i) &= \frac{\epsilon_0}{i\hbar} R_m \chi(\ell_s, \ell_i) A(\ell_s) A(\ell_i) \\ &\times C_p \check{T}_p(\omega_{\ell_s} + \omega_{\ell_i} - \omega_{p0}) \check{S}_p(\boldsymbol{\kappa}_{\ell_s} + \boldsymbol{\kappa}_{\ell_i}, 0) \\ &\times L \text{sinc}\left(\Delta K_m(\mathbf{k}_{\ell_s} + \mathbf{k}_{\ell_i}, \omega_{\ell_s} + \omega_{\ell_i}) \frac{L}{2}\right), \end{aligned} \quad (14)$$

where

$$\Delta K_m(\mathbf{k}, \omega) = k_z - k_{p0} - \frac{\omega - \omega_{p0}}{v_p} + \frac{|\boldsymbol{\kappa}|^2}{2k_{p0}} + m \frac{2\pi}{L}. \quad (15)$$

So far, we have explicitated in Eq.(8) and (9) the unnormalized state $|\psi\rangle$, of a photon-pair down-converted during a pump pulse. Its squared modulus $\langle\psi|\psi\rangle$ is the probability for such a down-conversion to effectively occur. The effect of spectral and spatial filtering on the photon-pair state is developed in the following section.

B. Spectral and spatial filtering

The calculation of the effect of filtering on one-photon states is detailed in Appendix B. Extrapolation to two-photon states is straightforward and only results are given here. Filters give rise to losses and two photon states are consequently transformed into mixed states, i.e. non coherent superpositions of two-photon, one-photon and zero-photon terms. In the case of coincidence counting, the two-photon state component is post-selected and we will discard zero- and one-photon terms.

Purely spectral filters are described by a function $\mathcal{F}(\omega - \omega_F)$ defining their amplitude transmission with a maximum normalized at 1 at their central frequency ω_F . More generally, a spectral filter can be sensitive to the direction of the wavevector (like prisms, gratings or Fabry-Pérot etalons), and it may be necessary to take a $\boldsymbol{\kappa}$ -dependence into account : $\mathcal{F}(\omega - \omega_F, \boldsymbol{\kappa})$.

Spatial filtering is modelled as the coupling of the down-converted field to a single spatial mode defined, in a medium of refractive index n' , by a frequency dependent function $\mathcal{O}_{\omega,0}(\mathbf{r})$. The filter location $z = z_0$ defines the transverse plane where the coupling is considered to take place. This coupling induces a state projection on the target mode, and the state of the transmitted photons is associated with a creation operator $\hat{\delta}_{\omega}^\dagger$.

Following Eq. (8), the spectrally-filtered, free-space two-photon state is given by

$$|\psi_0\rangle = \sum_{\ell_s, \ell_i} \gamma_0(\ell_s, \ell_i) \gamma_T^{(2)}(\ell_s, \ell_i) \hat{a}_{\ell_s}^\dagger \hat{a}_{\ell_i}^\dagger |0\rangle, \quad (16)$$

where

$$\gamma_T^{(2)}(\ell_s, \ell_i) = \mathcal{F}(\omega_{\ell_s} - \omega_{s_0}, \boldsymbol{\kappa}_{\ell_s}) \mathcal{F}(\omega_{\ell_i} - \omega_{i_0}, \boldsymbol{\kappa}_{\ell_i}), \quad (17)$$

and ω_{s_0} and ω_{i_0} are the signal and idler frequencies selected by the filters, which can be equal for degenerate down-conversion using a unique filter. The squared modulus of this state, $\langle\psi_0|\psi_0\rangle$, is the probability P_0 of generating a photon pair during a pump pulse in the filter bandwidth.

The spectrally and spatially filtered state is given by

$$|\psi_2\rangle = \sum_{\ell_s, \ell_i} \gamma_0(\ell_s, \ell_i) \gamma_T^{(2)}(\ell_s, \ell_i) \gamma_S^{(2)}(\ell_s, \ell_i) \hat{\delta}_{\omega_{\ell_s}}^\dagger \hat{\delta}_{\omega_{\ell_i}}^\dagger |0\rangle, \quad (18)$$

where

$$\begin{aligned} \gamma_S^{(2)}(\ell_s, \ell_i) &= \frac{1}{\mathcal{S}} \check{O}_{\omega_{\ell_s},0}^*(\boldsymbol{\kappa}_{\ell_s}, z_0) \check{O}_{\omega_{\ell_i},0}^*(\boldsymbol{\kappa}_{\ell_i}, z_0) \\ &\times e^{i(k'_{z,\ell_s} + k'_{z,\ell_i})z_0}, \end{aligned} \quad (19)$$

$\check{O}_{\omega,0}^*$ is the complex conjugate of the transverse Fourier transform of $\mathcal{O}_{\omega,0}$, $k'_{z,\ell} = k_{z,\ell} n'(\omega_\ell) / n(\omega_\ell)$ is the longitudinal wavevector evaluated in medium of refractive index n' , and \mathcal{S} is the transverse section of the quantization volume.

Due to spectral and spatial filtering, $|\psi\rangle$ has become $|\psi_2\rangle$. The squared modulus of this state, $\langle\psi_2|\psi_2\rangle$, is the probability P_2 that one pulse has generated a photon pair and that this pair has been transmitted by the spectral and spatial filters. Its numerical calculation is performed in subsection **II D**, using assumptions that will allow us to separate the frequency dependence from the wavevector dependence in Eq. (15) as shown in the next subsection.

C. Assumptions

A few assumptions are quite natural when aiming at applications in quantum information. Moreover, they enable further analytical development as well as faster numerical calculation. The consequent approximations, mostly used to simplify the expressions of ΔK in (19), aim at eventually decoupling the frequency dependence (ω) from the angular dependence ($\boldsymbol{\kappa}$) in the wavevectors \mathbf{k} .

1. Collinear collection

When using long crystals, as in most recent and efficient devices [41, 42], a collinear configuration is required. In such a case, the paraxial approximation, as already used for the pump beam, can be applied to the down-converted photons on the z -axis, giving the following expression for the longitudinal component of the signal wavevector

$$k_{zs} = k_{s_0} + \frac{\omega_s - \omega_{s_0}}{v_s} - \frac{1}{2} \frac{|\boldsymbol{\kappa}_s|^2}{|\mathbf{k}_s|}, \quad (20)$$

where k_{s_0} is the wavenumber of collinearly emitted signal photons at the central frequency of the filter ω_{s_0} , and $v_s = c/n_s$ with n_s the refractive index in the crystal at the signal frequency. A similar expression applies for k_{zi} .

2. Narrow bandwidth

When filtering limits the source bandwidth to less than a few nanometers ($\Delta\omega_F \ll \omega_{p_0}$), we have $\omega_s \approx \omega_{s_0}$ and $\omega_i \approx \omega_{i_0}$ in which case, according to Eq. (20), the phase mismatch ΔK depends only on $\boldsymbol{\kappa}_s, \boldsymbol{\kappa}_i$. The fields amplitudes and nonlinear susceptibility, respectively defined in Eqs. (2) and (6), can then be considered constant.

A narrow bandwidth is a desirable characteristic for long-distance communications, as it reduces dispersion in optical fibers and is also required for projects of repeaters based on quantum memories [3, 20]. In such memories based on atomic and ionic resonances, the acceptance bandwidth is lower than a few GHz [22], which definitely lies within the present assumption.

3. Spatial dependance of the nonlinear susceptibility

Although it is possible to calculate $\sum_m \gamma_{0m}$ for an arbitrary $R(z)$, this function is generally chosen so that one term $\gamma_{0\tilde{m}}$ is as high as possible and is the only optically phase-matched one. This is achieved by periodically poling the nonlinear susceptibility with a period Λ . In this case, \tilde{m} should be chosen such that $L = \tilde{m}\Lambda$, and $R_{\tilde{m}} = 2/\pi$, is the first term of the Fourier expansion of a square periodic function. In the following, we will consider the case of a collinear interaction in a periodically poled crystal with an effective susceptibility $\chi_{\text{eff}} = \chi(\omega_{s_0}, \omega_{i_0})2/\pi$, corresponding to specific polarizations of the pump, signal and idler beams. The case of the homogeneous crystal could also be described using an infinite period and $R_{\tilde{m}} = 1$.

4. Quasi-degenerate down-conversion

In the following, we will restrict the process to quasi-degenerate down-conversion, that is $|\delta\omega| \ll \omega_{p_0}$ with $\delta\omega = \omega_{s_0} - \omega_{i_0}$.

The phase mismatch then reduces to

$$\Delta K(\boldsymbol{\kappa}_s, \boldsymbol{\kappa}_i) \approx \Delta k_0 + \frac{|\boldsymbol{\kappa}_s + \boldsymbol{\kappa}_i|^2}{2k_{p_0}} - \left(1 - \frac{\delta\omega}{\omega_{p_0}}\right) \frac{n_p}{n_s} \frac{|\boldsymbol{\kappa}_s|^2}{k_{p_0}} - \left(1 + \frac{\delta\omega}{\omega_{p_0}}\right) \frac{n_p}{n_i} \frac{|\boldsymbol{\kappa}_i|^2}{k_{p_0}}, \quad (21)$$

where $\Delta k_0 = k_{s_0} + k_{i_0} - k_{p_0} + \frac{2\pi}{\Lambda}$ is the longitudinal phase mismatch. This together with the narrow bandwidth assumption allows for omitting the frequency dependence of the functions $\mathcal{O}_{\omega,0}$, describing the target mode. It can therefore be replaced by the unique function $\mathcal{O}_0 = \mathcal{O}_{\omega_{p_0}/2,0} \approx \mathcal{O}_{\omega_{s_0},0} \approx \mathcal{O}_{\omega_{i_0},0}$.

D. Figures of merit

In our general configuration of Fig. 1, only the spectrally and spatially filtered pairs with a probability P_2 will give rise to measured coincidences between the two channels. It is also important to be aware of the total brightness, accounting for all down-converted pairs in the spectral bandwidth under consideration P_0 . The pair coupling efficiency is defined as the ratio $\Gamma_2 = P_2/P_0$. This energetical figure of merit, however, cannot describe the loss of coherence due to spatial filtering, related to the ratio of coincidences to single counts. That is why we are interested in the probability $\Gamma_{2|1}$ to have the idler photon coupled to the target spatial mode when the signal is coupled to that mode (or vice versa). It is sometimes called heralding ratio or conditional efficiency, measuring the ability of one photon to herald its twin for single photon source applications. It is also very useful when the source is to be used as an entangled photon pair source

as a quality figure of merit. It will be evaluated using the single-photon coupling probability P_1 of having at least one photon transmitted by the filters. In the following subsections, a detailed calculation of each of these parameters is given.

1. Source brightness

The coincidental presence of both photons in the target spatial mode over a whole pulse duration is based on the two-photon state $|\psi_2\rangle$ (Eq. (18)) and is given by

$$P_2 = \langle \psi_2 | \psi_2 \rangle. \quad (22)$$

To make further calculations, we take the limit of an infinite quantization volume, in which sums over modes ℓ are replaced by integrals over the wavevectors \mathbf{k} in the usual way [43, 44] with discrete variables like \mathbf{k}_ℓ , ω_ℓ and operators like \hat{o}_{ω_ℓ} changed into their continuous counterparts \mathbf{k} , $\omega(\mathbf{k})$ and $\hat{o}(\omega(\mathbf{k}))$. Moreover, the narrow bandwidth assumption allows for calculating integrals over $\boldsymbol{\kappa}$ independently of integrals over ω , since $\boldsymbol{\kappa}$ mostly varies with the wavevector angle when ω is restricted to a small interval. Equation (22) gives, under the previous assumptions

$$P_2 = |C|^2 \Omega_2 K_2, \quad (23)$$

where

$$C = ie^{i(n'_s \omega_{s_0} + n'_i \omega_{i_0}) z_0 / c} \sqrt{\frac{\mathcal{E}_p \chi_{\text{eff}}^2 \omega_{s_0} \omega_{i_0}}{8 \epsilon_0 c^3 n_p n_s n_i}} \quad (24)$$

is a constant with n'_s (resp. n'_i) the refractive index in the medium where \mathcal{O}_0 describes the target mode.

The functions

$$\Omega_2 = \int \frac{d\omega_s}{2\pi} \int \frac{d\omega_i}{2\pi} \left| \check{T}_p(\omega_s + \omega_i - \omega_{p_0}) \times \mathcal{F}(\omega_s - \omega_{s_0}) \mathcal{F}(\omega_i - \omega_{i_0}) \right|^2 \quad (25)$$

and

$$K_2 = \left| \iint \frac{d^2 \boldsymbol{\kappa}_s}{(2\pi)^2} \iint \frac{d^2 \boldsymbol{\kappa}_i}{(2\pi)^2} \check{S}_p(\boldsymbol{\kappa}_s + \boldsymbol{\kappa}_i, 0) \times \check{\mathcal{O}}_0(\boldsymbol{\kappa}_s, z_0) \check{\mathcal{O}}_0(\boldsymbol{\kappa}_i, z_0) e^{-iz_0 \left(\frac{n_p}{n'_s} \frac{|\boldsymbol{\kappa}_s|^2}{k_{p_0}} + \frac{n_p}{n'_i} \frac{|\boldsymbol{\kappa}_i|^2}{k_{p_0}} \right)} \times L \text{sinc} \left(\frac{\Delta K(\boldsymbol{\kappa}_s, \boldsymbol{\kappa}_i) L}{2} \right) \right|^2 \quad (26)$$

describe respectively the spectral and spatial dependence of P_2 . They must be both maximized in order to optimize the brightness.

The function Ω_2 involves the coupling of the temporal dependence of the pump pulse with the spectral filters. It has the dimension of a frequency and can be interpreted as the effective source bandwidth. Using an adequate

change of variables, it can be written as a convolution of the three spectrally-dependent functions and, as such, it is maximum when the filters are tuned so as to satisfy the energy conservation $\omega_{s_0} + \omega_{i_0} = \omega_{p_0}$:

$$\Omega_2 = |\check{T}_p|^2 * |\mathcal{F}|^2 * |\mathcal{F}|^2(\omega_{s_0} + \omega_{i_0} - \omega_{p_0}) \quad (27)$$

In the following, we will assume that this energy conservation condition is satisfied.

The dimensionless function K_2 takes into account the spatial interferences caused both by phase matching and coupling to the target mode. Its maximization will require a numerical optimization (see III C 2).

The factor $|C|^2$ appears then as a spectral probability density.

2. Pair coupling efficiency

The pair coupling efficiency Γ_2 is the ratio of the spectrally and spatially filtered pair probability (source brightness) to the spectrally filtered pair probability (total brightness)

$$\Gamma_2 = \frac{P_2}{P_0}. \quad (28)$$

The total brightness is calculated from the spectrally filtered, free space state $|\psi_0\rangle$ defined by Eq. (16)

$$P_0 = \langle \psi_0 | \psi_0 \rangle. \quad (29)$$

Using the same method as for P_2 , Eq. (29) leads to

$$P_0 = |C|^2 \Omega_2 K_0, \quad (30)$$

where K_0 is a dimensionless function describing the spatial dependence and defined by

$$K_0 = \iint \frac{d^2 \boldsymbol{\kappa}_s}{(2\pi)^2} \iint \frac{d^2 \boldsymbol{\kappa}_i}{(2\pi)^2} \left| \check{S}_p(\boldsymbol{\kappa}_s + \boldsymbol{\kappa}_i, 0) \times L \text{sinc} \left(\frac{\Delta K(\boldsymbol{\kappa}_s, \boldsymbol{\kappa}_i) L}{2} \right) \right|^2. \quad (31)$$

The pair coupling efficiency is then equal to

$$\Gamma_2 = \frac{K_2}{K_0}. \quad (32)$$

3. Heralding ratio and single-photon coupling

Evaluating the heralding ratio requires calculating the single-photon coupling probability defined by

$$P_1 = \langle \psi_1 | \psi_1 \rangle \quad (33)$$

for the state

$$|\psi_1\rangle = \sum_{\ell_s, \ell_i} \gamma_0(\ell_s, \ell_i) \gamma_T^{(1)}(\ell_s) \gamma_S^{(1)}(\ell_s) \hat{o}_{\omega_{\ell_s}}^\dagger \hat{a}_{\ell_i}^\dagger |0\rangle, \quad (34)$$

where

$$\gamma_T^{(1)} = \mathcal{F}(\omega_{\ell_s} - \omega_{s_0}, \boldsymbol{\kappa}_{\ell_s}) \quad (35)$$

corresponds to a spectral filtering of the signal and no filtering for the idler [45], and

$$\gamma_S^{(1)} = \frac{1}{\sqrt{S}} \check{\mathcal{O}}_0^*(\boldsymbol{\kappa}_{\ell_s}, z_0) e^{ik'_{z, \ell_s} z_0} \quad (36)$$

describes the coupling of the signal photon only into the target single mode.

In the same way as for P_2 and P_0 ,

$$P_1 = |C|^2 \Omega_1 K_1, \quad (37)$$

where

$$\begin{aligned} \Omega_1 &= \int \frac{d\omega_s}{2\pi} \int \frac{d\omega_i}{2\pi} \left| \check{T}_p(\omega_s + \omega_i - \omega_{p_0}) \mathcal{F}(\omega_s - \omega_{s_0}) \right|^2 \quad (38) \\ K_1 &= \iint \frac{d^2 \boldsymbol{\kappa}_i}{(2\pi)^2} \left| \iint \frac{d^2 \boldsymbol{\kappa}_s}{(2\pi)^2} \check{S}_p(\boldsymbol{\kappa}_s + \boldsymbol{\kappa}_i, 0) \check{\mathcal{O}}_0(\boldsymbol{\kappa}_s, z_0) \right. \\ &\quad \left. \times e^{-iz_0 \frac{n_p}{n_s} \frac{|\boldsymbol{\kappa}_s|^2}{k_{p_0}}} L \operatorname{sinc} \frac{\Delta K L}{2} \right|^2. \quad (39) \end{aligned}$$

As K_2 , K_1 requires numerical computation, whereas Ω_1 reduces to

$$\Omega_1 = \int \frac{d\omega}{2\pi} |\mathcal{F}(\omega)|^2 \quad (40)$$

which is proportional to the filter bandwidth itself.

The heralding ratio i.e. the conditionnal probability to couple the second photon to the target mode when its twin has been coupled, is defined by

$$\Gamma_{2|1} = \frac{K_2}{K_1}. \quad (41)$$

It is useful to define also the single photon coupling efficiency

$$\Gamma_1 = \frac{K_1}{K_0}. \quad (42)$$

These two coefficients are related to the pair coupling efficiency in the following way

$$\Gamma_2 = \Gamma_{2|1} \Gamma_1. \quad (43)$$

Note that $\Gamma_2 \neq \Gamma_1^2$, because of the spatial correlation between the two photons, in the same way as, because of the energy correlation of the two photons, the calculation of Ω_2 involves a convolution rather than a product of the filtering functions of the signal and idler photons (see Eq. (27)).

In order to get a physical insight into these results and show how this description can be used as a predictive tool for the design and optimization of entangled photon pair sources, the following section is devoted to a numerical calculation corresponding to the particular case of the experiment described in Section IV.

III. NUMERICAL OPTIMIZATION OF A NARROW-BAND FIBERED SOURCE PUMPED BY A GAUSSIAN BEAM

A. Gaussian pump beam, Gaussian target mode

We assume the pump beam to be Gaussian with a waist radius w_0 and Rayleigh length z_R

$$S_p(\boldsymbol{\rho}, 0) = \sqrt{\frac{2}{\pi w_0^2}} e^{-|\boldsymbol{\rho}|^2/w_0^2} \quad (44)$$

$$\check{S}_p(\boldsymbol{\kappa}, 0) = \sqrt{2\pi w_0^2} e^{-|\boldsymbol{\kappa}|^2 w_0^2/4}. \quad (45)$$

Using the fact that $k_{p_0}/2 = z_R/w_0^2$, the phase matching function becomes

$$\begin{aligned} \Delta K &\approx \Delta k_0 + \frac{w_0^2}{4z_R} \left[|\boldsymbol{\kappa}_s + \boldsymbol{\kappa}_i|^2 \right. \\ &\quad \left. - 2 \left(1 - \frac{\delta\omega}{\omega_{p_0}} \right) \frac{n_p}{n_s} |\boldsymbol{\kappa}_s|^2 - 2 \left(1 + \frac{\delta\omega}{\omega_{p_0}} \right) \frac{n_p}{n_i} |\boldsymbol{\kappa}_i|^2 \right]. \quad (46) \end{aligned}$$

The target mode acting as a spatial filter is defined by the profile of a Gaussian mode at its waist of radius a_0 located at z_0 . This can be the transverse mode of a fiber or its image by a lens collection system

$$\mathcal{O}_0(\boldsymbol{\rho}, z_0) = \sqrt{\frac{2}{\pi a_0^2}} e^{-|\boldsymbol{\rho}|^2/a_0^2} \quad (47)$$

$$\check{\mathcal{O}}_0(\boldsymbol{\kappa}, z_0) = \sqrt{2\pi a_0^2} e^{-|\boldsymbol{\kappa}|^2 a_0^2/4}. \quad (48)$$

B. Nondimensionalization

The coincidence probability P_2 given by Eq. (23) can now be detailed. It is useful to separate the fixed parameters from the configuration of the experiment that can be optimized

$$P_2 = \frac{\mathcal{E}_p \chi_{\text{eff}}^2 L \Delta\omega_F \omega_{s_0} \omega_{i_0} \omega_{p_0}}{8\epsilon_0 c^4 n_s n_i} \cdot \frac{\Omega_2}{\Delta\omega_F}(\delta) \cdot \frac{K_2}{k_{p_0} L}(\xi, \alpha, \zeta, \varphi_0), \quad (49)$$

where $\Delta\omega_F$ is the filter bandwidth, and the terms $\Omega_2/\Delta\omega_F$ and $K_2/(k_{p_0} L)$ depend only on the experimental configuration described by the following dimensionless

parameters :

$$\delta = \frac{4 \ln 2}{\Delta t_p \Delta \omega_F} \quad (\text{relative pump bandwidth})$$

$$\xi = \frac{L}{2z_R} \quad (\text{pump focusing parameter})$$

$$\alpha = \frac{a_0}{w_0} \quad (\text{normalized target mode waist size})$$

$$\zeta = \frac{z_0}{L} \quad (\text{longitudinal collection offset})$$

$$\varphi_0 = \Delta k_0 L \quad (\text{longitudinal phase mismatch})$$

$$\varphi_s = \frac{w_0}{2} \kappa_s \quad (\text{normalized signal transverse wavevector})$$

$$\varphi_i = \frac{w_0}{2} \kappa_i \quad (\text{normalized idler transverse wavevector})$$

The parameter Δt_p is the pump pulse duration. Eq. (49), that will be used to calculate the pair coupling efficiency and the heralding ratio, has a particular importance in itself, as it quantifies the absolute coupled brightness and its dependence on various experimental parameters. It will be discussed and compared to other reported work in Sec. V. The following section is dedicated to the theoretical determination of the experimental configuration that maximizes this brightness.

C. Optimization of the source brightness

1. Spectral optimization

The optimisation of Eq. (25) must generally be made numerically, but the influence of the relative pump bandwidth δ can be developed in a fully analytical way if the pump temporal envelope and the spectral filters are both Gaussian

$$T_p(t) = \left[\frac{4 \ln 2}{\pi \Delta t_p^2} \right]^{\frac{1}{4}} e^{-2 \ln 2 t^2 / \Delta t_p^2} \quad (51)$$

$$\check{T}_p(\omega) = \left[\frac{\pi \Delta t_p^2}{\ln 2} \right]^{\frac{1}{4}} e^{-\omega^2 \Delta t_p^2 / (8 \ln 2)} \quad (52)$$

$$\mathcal{F}(\omega) = e^{-2 \ln 2 \omega^2 / \Delta \omega_F^2}, \quad (53)$$

where Δt_p and $\Delta \omega_F$ are full widths at half maximum intensity. The coincidence probability then depends on δ in the following way

$$\frac{\Omega_2}{\Delta \omega_F}(\delta) = \sqrt{\frac{\pi / (8 \ln 2)}{1 + \frac{\delta^2}{2}}} \quad (54)$$

This dependence of the spectral factor of the source brightness is plotted in Figure 2 as a function of the relative pump bandwidth. It shows that the maximum value is asymptotically reached when the pump beam is monochromatic. In this case, the joint probability

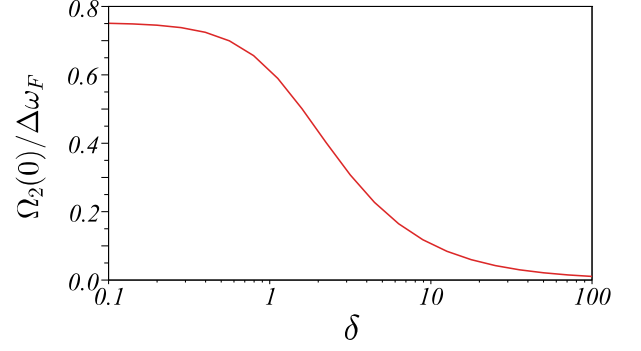


FIG. 2. Effect of the relative pump linewidth δ on the spectral transmission factor $\Omega_2/\Delta \omega_F$

for a photon and its twin to be transmitted is optimal. When the pump linewidth increases, some idler photons at $\omega_i = \omega_p - \omega_s$ and their corresponding signal photon at ω_s are not frequency-symmetric with respect to the filter center frequency ($\omega_p \neq \omega_{p_0}$), which is necessarily detrimental. This effect becomes significant for $\Delta \omega_p \geq \Delta \omega_F$ ($\delta \geq 1$). Although reducing the pulse duration Δt_p in order to increase the repetition rate does increase the effective photon pair rate, it is desirable to compromise in order to keep Ω_2 close to its maximum value.

2. Spatial optimization for degenerate down-conversion

In the following, we restrict ourselves to the case of a frequency-degenerate down-conversion ($\omega_s = \omega_i$), which corresponds to the experimental setup described in section IV. The dimensionless term to be optimized has the following expression

$$\frac{K_2}{k_{p_0} L}(\xi, \alpha, \zeta, \varphi_0) = \frac{8}{\pi^5} \xi \alpha^4 \left| \iint d^2 \varphi_s \iint d^2 \varphi_i Q_2 \right|^2 \quad (55)$$

with

$$\begin{aligned} Q_2 &= \exp \left\{ -|\varphi_s + \varphi_i|^2 \right\} \\ &\times \exp \left\{ -\alpha^2 (|\varphi_s|^2 + |\varphi_i|^2) \right\} \\ &\times \exp \left\{ -4\xi \zeta \left(\frac{n_p}{n'_s} |\varphi_s|^2 + \frac{n_p}{n'_i} |\varphi_i|^2 \right) \right\} \\ &\times \text{sinc} \left\{ \frac{\varphi_0}{2} + \xi \left[|\varphi_s + \varphi_i|^2 - 2 \frac{n_p}{n_s} |\varphi_s|^2 - 2 \frac{n_p}{n_i} |\varphi_i|^2 \right] \right\} \end{aligned} \quad (56)$$

Using polar coordinates, we can use the following mapping :

$$\begin{aligned} &\iint d^2 \varphi_s \iint d^2 \varphi_i Q_2 \\ &\longrightarrow 2\pi \int_0^\infty \rho_s d\rho_s \int_0^\infty \rho_i d\rho_i \int_0^{2\pi} d(\theta_s - \theta_i) Q'_2 \end{aligned} \quad (57)$$

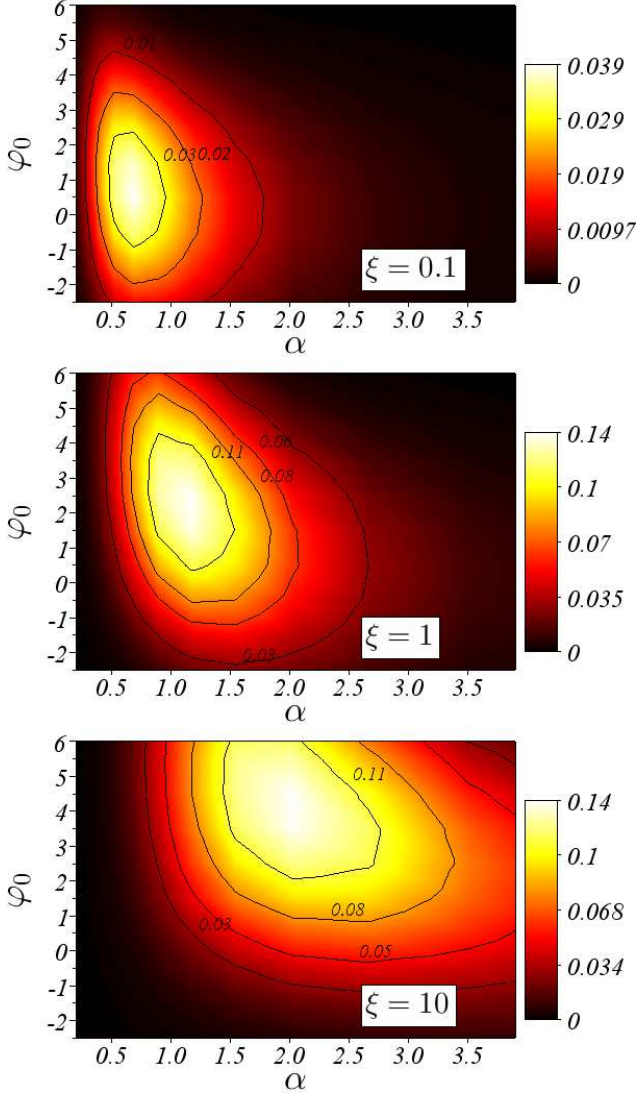


FIG. 3. Optimization of the spatial filtering factor $K_2/(k_{p_0}L)$ with respect to the normalized target mode waist α and the longitudinal phase mismatch φ_0 for three values of the focusing parameter : $\xi = 0.1$ (a) , $\xi = 1$ (b) , $\xi = 10$ (c) .

, with

$$\begin{aligned}
 Q'_2 = & \exp \left\{ - (1 + \alpha^2) (\rho_s^2 + \rho_i^2) \right\} \\
 & \times \exp \left\{ - 2\rho_s \rho_i \cos(\theta_s - \theta_i) \right\} \\
 & \times \exp i \left\{ - 4\xi \zeta \left(\frac{n_p}{n'_s} \rho_s^2 + \frac{n_p}{n'_i} \rho_i^2 \right) \right\} \\
 & \times \text{sinc} \left\{ \frac{\varphi_0}{2} + \xi \left[\left(1 - 2\frac{n_p}{n_s} \right) \rho_s^2 + \left(1 - 2\frac{n_p}{n_s} \right) \rho_i^2 \right. \right. \\
 & \quad \left. \left. + 2\rho_s \rho_i \cos(\theta_s - \theta_i) \right] \right\}. \quad (58)
 \end{aligned}$$

In this way, the quadruple integral turns into a triple integral which is numerically evaluated using an adaptive 3D quadrature algorithm [46].

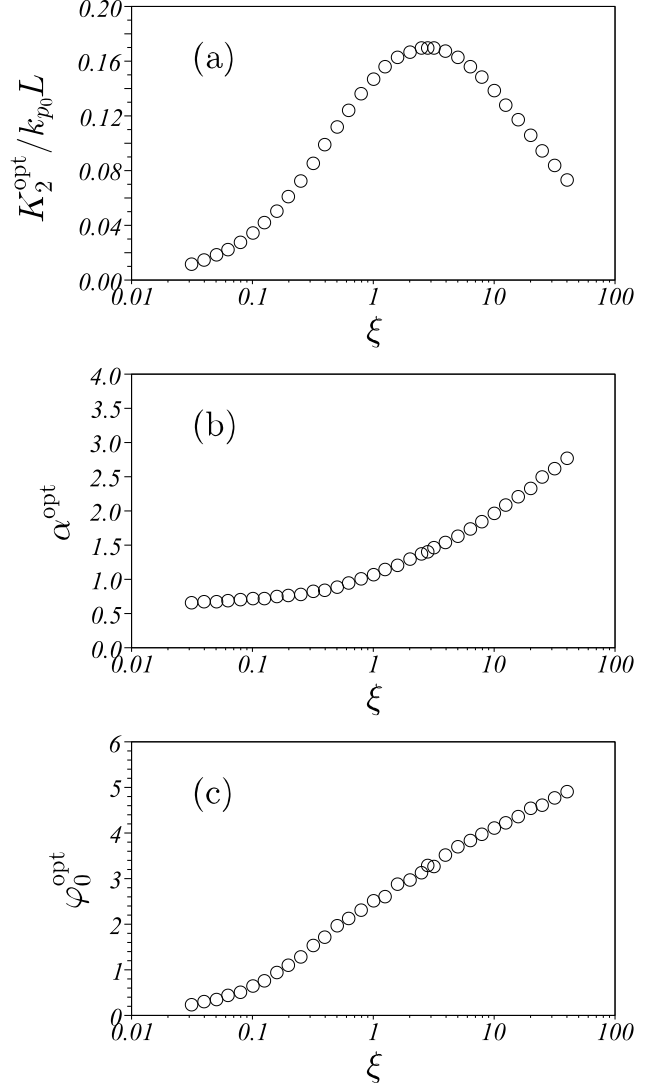


FIG. 4. Maximal value of the spatial filtering factor $K_2/(k_{p_0}L)$ (a) and associated optimal values of the normalized target mode waist α (b) and the longitudinal phase mismatch φ_0 (c), for various values of the focusing parameter ξ .

Figure 3 represents, for three different focusing parameters ξ , the value of the spatial filtering term $K_2/(k_{p_0}L)$ as a function of parameters α and φ_0 . It shows that there exists a unique couple $(\alpha^{\text{opt}}, \varphi_0^{\text{opt}})$ that allows reaching the maximum $K_2^{\text{opt}}/(k_{p_0}L)$ for a given value of ξ . Moreover, that maximum varies with ξ and the accuracy of $(\alpha^{\text{opt}}, \varphi_0^{\text{opt}})$ is found to be more critical for low ξ . Indeed, when the focusing of the pump beam increases, phase matching can only be satisfied in an average way, because of the large range of emitted angles, and α^{opt} results from a compromise between collecting weakly divergent photons with high efficiency and reducing this efficiency to collect more strongly divergent photons. Optimizing the pump beam for photon pair collection indeed

consists in finding the focusing parameter for which these two compromises offer the best performance.

Note that in Figure 3, the normalized longitudinal offset of single-mode collection ζ has been set to zero. We have checked that this choice gives optimal results. The optimality of $\zeta = 0$ is due to the symmetry of the problem in our particular choice of a Gaussian pump beam and Gaussian target spatial mode ; this might not be the case in other circumstances.

In order to find the focusing parameter ξ that gives rise to the highest collected brightness $K_2^{\text{opt}}/(k_{p_0}L)$, we have performed optimizations similar to that of Fig. 3 for values of ξ ranging from 0.03 to 40, that is for waist radiuses from ~ 200 to $\sim 5 \mu\text{m}$ for a red pump in common crystals, for instance. Knowing that $\zeta = 0$ is optimal in the whole range, we have plotted on Fig. 4 the values $K_2^{\text{opt}}/(k_{p_0}L)$, α^{opt} and φ_0^{opt} as a function of ξ .

According to Fig. 4b, the optimum normalized target mode waist α^{opt} does not vary very much over this large range of focusing parameters. Starting with an approximate matching of the target mode to the pump waists $\alpha^{\text{opt}} \approx 1$ at low focusing, our calculations exhibit a slow increase, showing that when focusing gets stronger, it is preferable to collect the weakly divergent photon pairs, since modes of larger waist sizes have smaller numerical apertures. On Fig. 4c, the optimum longitudinal phase mismatch φ_0^{opt} increases with the focusing parameter, as to compensate for the transverse mismatch caused by the strong focusing.

Fig. 4a shows that the value of the focusing parameter giving the highest value of $K_2^{\text{opt}}/(k_{p_0}L)$ is $\xi = 2.84$, for which the longitudinal phase mismatch is $\varphi_0 = 3.2$. These values correspond to the Boyd and Kleinman conditions [47] for a highest second harmonic generation efficiency with Gaussian beams. Indeed, when evaluating the brightness produced in a single Gaussian mode, the collinear degenerate down-conversion is a process symmetric to second harmonic generation.

However, down-converted photons are not entirely produced in a single mode. That is why it is important to investigate the optimization of the pair coupling efficiency Γ_2 defined in Eq. (28).

D. Optimization of the pair coupling efficiency

The total source brightness must also be calculated, using the dimensionless variables defined previously :

$$P_0 = \frac{\mathcal{E}_p \chi_{\text{eff}}^2 L \Delta\omega_F \omega_{s_0} \omega_{i_0} \omega_{p_0}}{8\epsilon_0 c^4 n_s n_i} \cdot \frac{\Omega_2}{\Delta\omega_F}(\delta) \cdot \frac{K_0}{k_{p_0}L}(\xi, \varphi_0), \quad (59)$$

where

$$\frac{K_0}{k_{p_0}L} = \frac{2}{\pi^3} \xi \iint d^2\varphi_s \iint d^2\varphi_i |Q_0|^2, \quad (60)$$

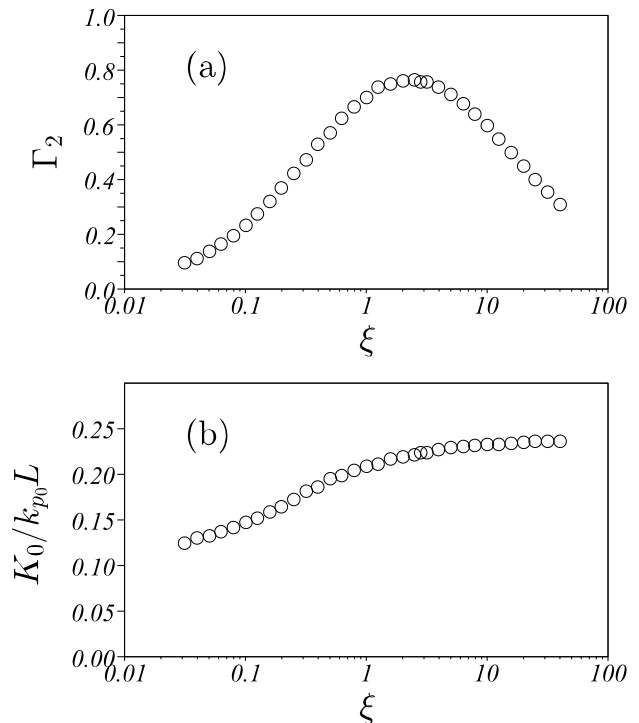


FIG. 5. Pair coupling efficiency Γ_2 (a) compared to the spatial factor $K_0/(k_{p_0}L)$ of the pair production probability (b), for various values of the focusing parameter ξ . $K_0/(k_{p_0}L)$ is evaluated for the longitudinal phase mismatch φ_0 that maximizes Γ_2 .

with

$$Q_0 = \exp \left\{ -|\varphi_s + \varphi_i|^2 \right\} \times \text{sinc} \left\{ \frac{\varphi_0}{2} - \xi \left[|\varphi_s + \varphi_i|^2 - 2\frac{n_p}{n_s}|\varphi_s|^2 - 2\frac{n_p}{n_i}|\varphi_i|^2 \right] \right\} \quad (61)$$

which can also be reduced to a 3D-integral.

The pair coupling efficiency Γ_2 (Eq. (32)) is calculated using Eqs. (55) and (60). It is plotted in Figure 5a, along with the dimensionless $K_0/(k_{p_0}L)$ proportional to the total brightness P_0 (Fig. 5b), as a function of the focusing parameter ξ . The total brightness does not vary much for $\xi \gtrsim 1$, therefore the coupling efficiency follows the same tendency as the single-mode brightness (Fig. 4a). However, the precise optimal value of ξ is no longer $\xi = 2.84$ but is closer to 2. For a red pump in common crystals, this means a waist radius difference of 20 %. Under different assumptions from the ones considered in this section, however, the difference might be greater. When power efficiency is critical, as for sources intended to be compact, it can be useful to have in mind that to collect most of the generated photons, optimizing on the mere source brightness is not optimal with respect to pump power consumption.

E. Optimization of the heralding ratio

The heralding ratio $\Gamma_{2|1}$ (Eq. (41)) requires the computation of the single-photon coupling probability P_1 , (cf. Eq. (37)) :

$$P_1 = \frac{\mathcal{E}_p \chi_{\text{eff}}^2 L \Delta\omega_F \omega_{s_0} \omega_{i_0} \omega_{p_0}}{8\epsilon_0 c^4 n_s n_i} \cdot \frac{\Omega_1}{\Delta\omega_F}(\delta) \cdot \frac{K_1}{k_{p_0} L}(\xi, \alpha, \zeta, \varphi_0), \quad (62)$$

where $\frac{\Omega_1}{\Delta\omega_F}$ only depends on the shape of the filter itself and where

$$\frac{K_1}{k_{p_0} L} = \frac{4}{\pi^4} \xi \alpha^2 \left| \iint d^2\varphi_s \left| \iint d^2\varphi_i Q_1 \right|^2 \right|, \quad (63)$$

with

$$\begin{aligned} Q_1 = & \exp \left\{ -|\varphi_s + \varphi_i|^2 \right\} \\ & \times \exp \left\{ -\alpha^2 |\varphi_s|^2 \right\} \\ & \times \exp \left\{ i \left[-4\xi \zeta \frac{n_p}{n_s} |\varphi_s|^2 \right] \right\} \\ & \times \text{sinc} \left\{ \frac{\varphi_0}{2} - \xi \left[|\varphi_s + \varphi_i|^2 - 2\frac{n_p}{n_s} |\varphi_s|^2 - 2\frac{n_p}{n_i} |\varphi_i|^2 \right] \right\} \end{aligned} \quad (64)$$

which can be reduced to a 3D-integral as for Q_2 and Q_0 .

The heralding ratio $\Gamma_{2|1} = K_2/K_1$ is plotted in Fig. 6 as a function of parameters α and φ_0 for three values of the focusing parameter $\xi = 0.1, 1, 10$. Contrary to the brightness depicted in Fig 3, the heralding ratio can reach a value close to 1 on the whole range of ξ . A large range of φ_0 is compatible with this maximum, but the overlap with the range leading to a high brightness is small. On the contrary, the tolerance on α is relatively low. When the results of P_2 and $\Gamma_{2|1}$ are both taken into account, the theory gives indeed useful information about the target mode waist for which the collection should be optimized with respect to φ_0 (through the crystal temperature), to find the best compromise between the brightness and the heralding ratio.

The details of an experiment that enabled a validation of our model is given in the following section.

IV. EXPERIMENTAL VALIDATION

A. Experimental setup

The experimental setup used to validate the theory is depicted in Fig. 7. SPDC is generated by focusing a pulsed pump beam at 782 nm in a periodically poled lithium niobate (PPLN) crystal of length $L = 2$ cm with a poling period $\Lambda = 19.34\mu\text{m}$. The mean pump power is 5 mW and the 25 ns Gaussian pulses (FWHM) are Fourier transform limited with a 2 MHz repetition rate. The spatial profile of the pump beam is also Gaussian. On-axis fluorescence around 1564 nm is collected into a telecom optical fiber through the lenses L_c (achromatic

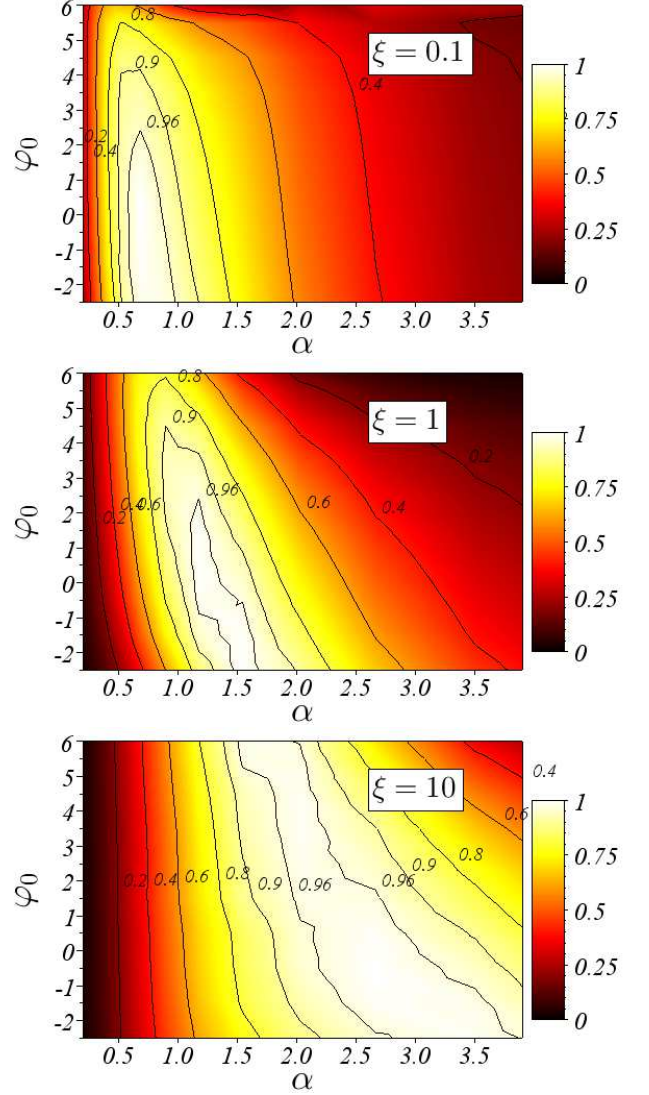


FIG. 6. Optimization of the heralding ratio $\Gamma_{2|1}$ with respect to the normalized target mode waist α and the longitudinal phase mismatch φ_0 for three values of the focusing parameter : $\xi = 0.1$ (a) , $\xi = 1$ (b) , $\xi = 10$ (c).

doublet) and L_i (asphere). The same low bandwidth filter ($\Delta\omega_F = 2\pi \times 75$ GHz) is used for both signal and idler photons so that the source is operated at the degeneracy frequency ($\omega_{s_0} = \omega_{i_0} = \omega_{p_0}/2$). A balanced coupler is used to split photon pairs with 50 % efficiency and the photons are detected on paths A and B.

B. Experimental method

In order to explain how the heralding ratio $\Gamma_{2|1}$ can be determined experimentally, let us show its relation to measured parameters :

$$\Gamma_{2|1} = \frac{K_2}{K_1} = \frac{\Omega_1 P_2}{\Omega_2 P_1}. \quad (65)$$

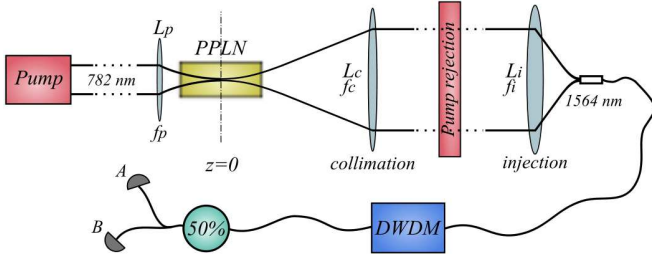


FIG. 7. Experimental setup : A pulsed pump laser at wavelength 782 nm is focused in a periodically-poled lithium niobate crystal (PPLN) with a lens L_p of focal length f_p . Down-converted photons at 1564 nm are coupled into an single mode fiber through an optical system composed of lenses L_c and L_i of respective focal lengths f_c and f_i . Spectral filtering is performed via a DWDM add-drop filter of bandwidth 75 GHz, and photons are split with 50 % efficiency towards detectors A and B using a balanced fibered coupler.

The experimental parameter P_{AB} corresponding to the calculated P_2 is the measured coincidence probability per pulse from which accidental and noise coincidences are subtracted, and P_1 is related to the measured counts on channel I from which dark counts have been subtracted :

$$P_{AB} = \mathcal{T}_A \mathcal{T}_B P_2 \quad P_I = \mathcal{T}_I P_1 \quad (66)$$

where \mathcal{T}_I is the overall transmission of channel I . We obtain :

$$\Gamma_{2|1} = \frac{\Omega_1}{\Omega_2} \frac{P_{AB}}{\mathcal{T}_A \mathcal{T}_B} \frac{\mathcal{T}_I}{P_1} \quad (67)$$

The heralding ratio $\Gamma_{2|1}$ can hence be determined from the measurements of counts and coincidences, provided the insertion losses have been previously determined [48]. It is then possible to validate its dependence with respect to the pump focusing parameter ξ and the normalized target mode waist α .

The variation of ξ was obtained by changing the lens L_p focusing the pump beam into the PPLN crystal. For each value of the focal length f_p , the waist of the pump beam was measured, allowing the determination of z_R and $\xi = L/(2z_R)$.

Counts and coincidences were then measured using various focal lengths f_i of the lens focusing the SPDC beam into the fiber. The value a_0 of the image of the fiber waist in the crystal was determined using the magnification factor f_c/f_i of the collection system (composed of the lenses L_c and L_i) in order to determine $\alpha = a_0/w_0$. Let us note that each data point requires changing the focusing lens, realigning the setup, and successively optimizing the collection with at least five different injection lenses, with the phase mismatch (crystal temperature) as an additional degree of freedom.

C. Experimental results

The experimentally determined $\Gamma_{2|1}$ can then be compared to its theoretical value when the normalized target mode waist α is varied. Figure 8 shows two examples : the pump focusing is kept constant with $f_p = 100$ mm ($\xi = 0.76$, Fig. 8a) or $f_p = 50$ mm ($\xi = 2.7$, Fig. 8b). $\Gamma_{2|1}$ is normalized and plotted as a function of α for $\zeta = 0$ and the adequate value of the remaining unknown dimensionless parameter φ_0 is found by horizontally fitting the theoretical curve to the experimental data. For $\xi = 0.76$, φ_0 is found to be around 2.0 while it is around 3.2 for $\xi = 2.7$. These values of φ_0 are also in agreement with the theoretical predictions corresponding to the brightness optimization. Indeed, although each plotted values of $\Gamma_{2|1}$ was obtained after optimizing this figure of merit itself, the experimental starting point was a preliminary optimization around a maximum source brightness. When $\Gamma_{2|1}$ and P_2 have a common optimum in the (α, φ_0) space, it is not surprising to converge close to $(\alpha^{\text{opt}}, \varphi_0^{\text{opt}})$ (optimum of P_2 as shown in Fig. 4 as a function of ξ) when optimizing with respect to $\Gamma_{2|1}$.

The very good agreement of our theory with the experimental results confirms its validity. For practical applications it is remarkable that only the measurement of the pump waist is required for the optimization of the SPDC source, the choice of the collection magnification being directly derived from the calculations presented in our analysis, which leaves the remaining parameter φ_0 to a heuristic, using the mere crystal temperature.

The absolute value of the heralding ratio was also derived from the preliminary measurements of $il_A = 0.026$ and $il_B = 0.024$. In Fig. 9a, the experimental absolute value of the heralding ratio $\Gamma_{2|1}$ is plotted as a function of the focusing parameter ξ . The result is almost constant, as predicted by the theory, but around 30 % below the expected optimal value that is close to 100 %. This difference is probably due to imperfections in the Gaussian pump beam and aberration in the optical system used to eliminate pump photons and to collect down-converted photon pairs into the fiber.

Let us also remark that the maximum measured value of $\Gamma_{2|1} = 0.7$, although not optimal, is to our knowledge impossible to reach by coupling PPLN waveguides into single-mode fibers, due to the mode mismatch between the rectangular profile of the guided mode and that - circular- of a fiber. This makes focused SPDC in bulk crystals probably more suitable than waveguide crystals when a high state fidelity is critical and limited by other constraints. For instance, the complex spectral filtering required for quantum memories associated with its limited storage-retrieval efficiency makes the coupling efficiency a parameter that is more than ever desirable to maximize.

In summary, we have confirmed 1) the dependence of the heralding ratio on the target mode size, 2) its quasi-independence on the focusing parameter, and 3) that our theory predicts with a very good precision the optimal

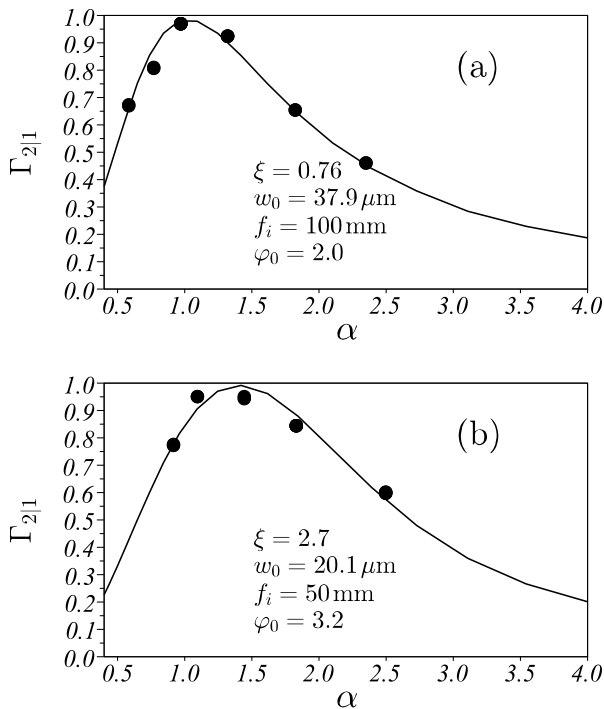


FIG. 8. Comparison of theoretically (solid lines) vs. experimentally (dots) determined heralding ratio $\Gamma_{2|1}$, as a function of the normalized target mode waist α for two different focusing parameters : $\xi = 0.76$ (a) and $\xi = 2.7$ (b).

target mode size for a particular focusing parameter.

V. DISCUSSION

A. Comparison with other works

As mentioned in the introduction, our work covers issues that were addressed by other authors with various assumptions or methods. The two figures of merit that can provide a relevant comparison are the absolute brightness and the coupling efficiency. We will also discuss a few reported experimental validations.

About the absolute brightness, Ling *et al.* [49] were among the first to propose an expression of the absolute photon pair rate collected into a single Gaussian spatial mode. Apart from the fact that they consider the case of a continuous pump ($\delta = 0$), our calculations are consistent dimension-wise. Moreover, everything else being equal, a spatial filtering factor can be identified in their analysis: its dependence with the focusing parameter and the longitudinal phase mismatch is of the form $\xi \text{sinc}^2(\varphi_0/2)$, which is indeed the result we find for the specific case of low focusing ($\xi \ll 1$) and $\alpha = \sqrt{2}$, corresponding to Ling's assumptions : thin crystal, negligible pump diffraction, equal Rayleigh lengths for pump and down-converted photons. However, under our less

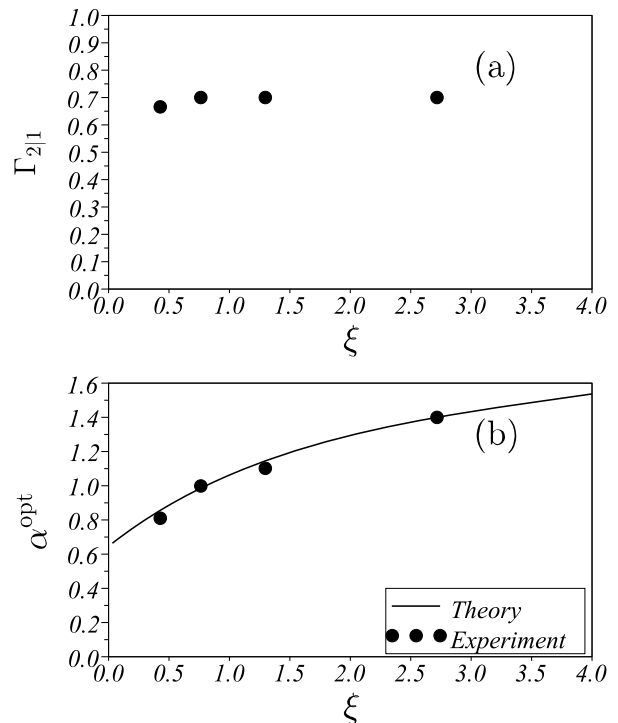


FIG. 9. (a) Measured heralding ratio $\Gamma_{2|1}$ plotted for 4 focal lengths $f_p = 150, 100, 75, 50 \text{mm}$, as a function of the focusing parameter $\xi = 0.44, 0.76, 1.05, 2.70$. (b) Corresponding experimental (circles) and calculated (solid line) value of the normalized target mode waist α for each value of $\Gamma_{2|1}$

restrictive assumptions, we have shown that $\alpha = \sqrt{2}$ is optimal for $\xi = 2.84$, whereas for low focusing, $\alpha \leq 1$.

More recently, the absolute value of the source brightness was calculated by Mitchell [37] in the Heisenberg picture, under assumptions similar to ours. This investigation has been restricted to a monochromatic, continuous pump field, and a direct expansion of the Hamiltonian onto the target Gaussian modes was performed, as opposed to our choice of investigating the single-mode coupling of free-space expanded fluorescence in the interaction picture. Our theory, which is developed in the Schrödinger picture, is nevertheless fully consistent with the results of Mitchell and we suggest in the next subsection how to generalize it using the same framework.

As for the coupling efficiency issue, let us recall that we investigated two parameters : the pair collection efficiency and the heralding ratio. Our results concerning the pair collection efficiency are consistent with that of Bennink [38], who found a linear dependence on the crystal length when the source bandwidth is much smaller than the phase-matching bandwidth, as opposed to Ljunggren *et al.* [35] who conclude on a \sqrt{L} -dependence. Let us point out that, as Bennink [38], we have taken into account the diffracting nature of the pump beam, and considered the longitudinal phase mismatch as a degree of freedom for optimization. As a

result, our optimization of Γ_2 for Gaussian beams at the degenerate frequency is optimal close to the well-known Boyd & Kleinman conditions [47] : $\xi = 2.84$, $\varphi_0 = 3.2$ and equal Rayleigh length for the pump and down-converted photons ($\alpha = \sqrt{2}$). An advantage of our framework is that the particular pump and target modes, filter shape, pump linewidth, etc. are only used in the very last step of the optimization, *i.e.* the computation of a multiple integral. Up to then, our framework remains very general.

As far as the heralding ratio is concerned, as opposed to the coupled brightness, it is found to be close to 1 whatever the focusing strength, provided the target mode waist α and phase mismatch φ_0 are adjusted according to our theory. Interestingly, a subset of (α, φ_0) which maximizes the heralding ratio is generally close to the optimal brightness, giving the configuration for an optimal general source performance. This conclusion is different from that of Bennink [38] who finds that a strong reduction of brightness is necessary to achieve a high heralding ratio, highlighting what could be a fundamental trade-off for single-mode applications. This apparent disagreement could be due to our specific narrow-band assumption. Our experiments confirm that the narrow-band behaviour follows our predictions, which is a positive result as far as the perspectives of SPDC for narrow-band applications are concerned.

As remarked by Bennink, very few among the reported theoretical works have been experimentally validated, probably because of the complexity of such experiments that involve multiple parameters to optimize simultaneously and to measure precisely. Reported experiments were realized for a single set of non-optimal parameters [35] or in a configuration which is not in the scope of our theory [34]. Thanks to a careful reduction of systematic errors, our experimental results show that our model could be used in order to optimize the experimental source configuration.

B. Extension to other source designs

Although the calculation done in Sec. III uses a bulk periodically-poled crystal pumped with a single-mode diffractive gaussian pump beam, as required for successful comparison with our experiment, the general theoretical framework of Sec. II can be applied to other source designs. A few examples are given hereafter.

First, it is straightforward to correct the results for non-degenerate down conversion, provided the frequency difference is small compared to the pump frequency.

It is also possible to use a non-gaussian pump or target mode profile, by changing the functions S_p and \mathcal{O}_0 respectively. If required, a second dimensionless parameter can be introduced apart from α in order to characterize the mode ellipticity. In this case, the 4D- to 3D-integral reduction used in Eq. (57) is impossible due to the absence of cylindrical symmetry, making the computation

longer. Let us note that for such high-dimensions integrals, a Monte-Carlo integration method could give faster results.

As far as the crystal type is concerned, as mentioned at the end of Sec. II A, a non-periodically or multi-periodically poled crystal can be used by coherently summing the first N components of the Fourier series expansion of the non-linear susceptibility $\overline{\chi}^{(2)}(z)$. When $\overline{\chi}^{(2)}(z)$ is not of high complexity, the expansion can be truncated to a low N , making the calculation not much more time-consuming.

SPDC sources using a periodically-poled crystal with integrated waveguide are also commonly used. The coupling of photons down-converted in such devices could be modelled using our framework, by slicing the crystal into N sub-crystals, for each of which the state coupled to the waveguide mode is calculated. For a slice $j = 1 \cdots N$ centered on z_j , the target mode is assumed to have its waist located at z_j . If diffraction is taken into account as in the case of bulk crystals, the pump profile $S_p(\rho, z_j)$ differs in each slice according to Eq. (10). However, the pump field is generally also guided in the integrated waveguide and the pump profile should be chosen constant, which is done by removing the diffraction term in Eq. (10). The final state for which figures of merit like brightness or heralding ratio are evaluated results from coherently summing the states originating from each slice, taking into account their respective phases.

Let us remark that, in integrated waveguides designed to be single-mode for down-converted photons, the pump field is generally spatially multimode. This can also be taken into account by replacing the single-mode pump function S_p by a mode expansion $\sum_{j=1}^N S_{p_j}$. As for a general nonlinear susceptibility distribution, this only increases the computation time by a factor N , which can be chosen according to the desired precision.

VI. CONCLUSION

In this paper, we have calculated the state of a photon pair produced by a narrow-band spontaneous parametric down-conversion (SPDC) source with arbitrary pump spatial and temporal profile, and arbitrary filtering configuration.

When applied to Gaussian modes, our theory is consistent with the most recently reported work where realistic assumptions have been made. Within our assumptions, no incompatibility is observed between a high brightness and a high heralding ratio. We believe this result could increase the interest of SPDC sources for narrow-band quantum information applications.

Once validated under the Gaussian assumptions, our theoretical framework, which allows an extensive study of the source through many degrees of freedom, should allow the prediction of the best performance for more original source designs, including non-Gaussian pump and target

modes, guided or diffractive, single or multi-mode, with arbitrary nonlinear susceptibility longitudinal distribution.

ACKNOWLEDGMENTS

This work is a part of the project ‘‘embryonic Quantum Network’’, funded by the ‘‘Agence Nationale pour la Recherche’’.

Appendix A: Conventions for Fourier transforms and convolutions

All along this paper, we use the following Fourier transform conventions :

$$\begin{aligned}\check{f}(\omega) &= \int dt e^{i\omega t} f(t) \longleftrightarrow f(t) = \int \frac{d\omega}{2\pi} e^{-i\omega t} \check{f}(\omega) \\ \check{f}(\mathbf{k}) &= \int d^3\mathbf{r} e^{-i\mathbf{k}\cdot\mathbf{r}} f(\mathbf{r}) \longleftrightarrow f(\mathbf{r}) = \int \frac{d^3\mathbf{k}}{(2\pi)^3} e^{i\mathbf{k}\cdot\mathbf{r}} \check{f}(\mathbf{k})\end{aligned}$$

f is normalized if :

$$\begin{aligned}\int dt |f(t)|^2 &= \int \frac{d\omega}{2\pi} |\check{f}(\omega)|^2 = 1 \\ \int d^3\mathbf{r} |f(\mathbf{r})|^2 &= \int \frac{d^3\mathbf{k}}{(2\pi)^3} |\check{f}(\mathbf{k})|^2 = 1\end{aligned}$$

Convolutions are defined as follows :

$$\begin{aligned}f * g(t) &= \int dt' f(t')g(t - t') \\ f * g(\mathbf{r}) &= \int d^3\mathbf{r}' f(\mathbf{r}')g(\mathbf{r} - \mathbf{r}') \\ \check{f} * \check{g}(\omega) &= \int \frac{d\omega'}{2\pi} \check{f}(\omega')\check{g}(\omega - \omega') \\ \check{f} * \check{g}(\mathbf{k}) &= \int \frac{d^3\mathbf{k}'}{(2\pi)^3} \check{f}(\mathbf{k}')\check{g}(\mathbf{k} - \mathbf{k}')\end{aligned}$$

Appendix B: Spatial and spectral filtering

In this appendix we describe the effect of filters on a single photon state. Generalization to the case of photon pairs is made in Section II B.

Although the action of filters will be described in the Fourier space, they are located at a particular position of the setup and a specific time lag $[t_0, t_1]$ can be defined such that when $t < t_0$, the photon state is completely unaffected by the filter yet and when $t > t_1$, the effect of the filter on the photon state has been completed. After having introduced some tools in the first two sections, we will successively examine how spectral and spatial filters change a state $|\Psi(t_0)\rangle$ into a state $|\Psi(t_1)\rangle$.

1. ‘‘Localized’’ photonic states and pseudo-wavefunction

In this paper, we sometimes use localized photonic states introduced by L. Mandel [50]. Based on plane-wave states $|1_{\mathbf{k}}\rangle$ in a quantization volume \mathcal{V} , a state describing a photon localized around \mathbf{r} is defined by :

$$|1_{\mathbf{r}}\rangle = \sum_{\mathbf{k}} \frac{e^{-i\mathbf{k}\cdot\mathbf{r}}}{\sqrt{\mathcal{V}}} |1_{\mathbf{k}}\rangle \quad (\text{B1})$$

Then, a general photon state $|\psi\rangle = \sum_{\mathbf{k}} \psi_{\mathbf{k}} |1_{\mathbf{k}}\rangle$ can be written as

$$|\psi\rangle = \int_{\mathcal{V}} d^3\mathbf{r} \psi(\mathbf{r}) |1_{\mathbf{r}}\rangle \quad (\text{B2})$$

where $\psi(\mathbf{r})$ is a spatial pseudo-wavefunction for which $\psi_{\mathbf{k}}$ are the coefficients of its Fourier series expansion in the quantization volume \mathcal{V} . Such a wavefunction is only valid provided the volume V in which the localization probability $P(V)$, defined as follows, is evaluated is large enough (each dimension much larger than the wavelength) :

$$P(V) = \int_{\mathcal{V}} d^3\mathbf{r} |\langle 1_{\mathbf{r}} | \psi \rangle|^2 = \int_{\mathcal{V}} d^3\mathbf{r} |\psi(\mathbf{r})|^2 \quad (\text{B3})$$

This probability is naturally equal to unity in the quantization volume :

$$P(\mathcal{V}) = \int_{\mathcal{V}} d^3\mathbf{r} |\psi(\mathbf{r})|^2 = \langle \psi | \psi \rangle = \sum_{\mathbf{k}} |\psi_{\mathbf{k}}|^2 = 1. \quad (\text{B4})$$

2. Spatial filtering

a. Principle

A spatial filter located on the propagation axis at $z = z_0$ is modelled as the coupling in the plane $z = z_0$ of the down-converted field into a single spatial mode defined by a function $\mathcal{O}_{\omega,0}(\mathbf{r})$. The index ω indicates that this spatial mode can be frequency-dependent for a given filter.

Note that z_0 may be in $[-L/2, L/2]$. As an example, if the spatial filtering is done via an optical fiber, the effective location of the filter is where the lens collection system images the entrance of the fiber.

To evaluate its transmitted component, the down-converted field initially described as a superposition of plane waves is better expanded on a particular set of orthogonal modes $\{\mathcal{O}_{\omega,j}(\mathbf{r})\}$, one of which ($\mathcal{O}_{\omega,0}(\mathbf{r})$) being the spatial mode selected by the considered filter.

If coupled to other modes, photons are supposed to be lost. As for spectral filtering, this leads to a mixed state.

For instance, the fundamental mode can be the Gaussian mode of the Laguerre-Gauss basis, suited to single-mode fibers. Then $\mathcal{O}_{\omega,j=0}(\mathbf{r})$ describes a Gaussian beam of waist size equal to the field radius of a fiber mode.

If the image of the fiber entrance is located at $z = z_0$, $\mathcal{O}_{\omega,j=0}(\boldsymbol{\rho}, z_0)$ describes the Gaussian beam waist profile corresponding to the fiber transverse mode.

A projection at $z = z_0$ into that single mode selects the photon state component which is transmitted by the filter. Once transmitted, the state is said to be in the spatial mode characterized by the annihilation operator \hat{o}_ω . Let us note that whether the spatial mode for $z \geq z_0$ continues to be that of a Gaussian beam (as for a cavity) or is actually described by a guided propagation with a constant transverse profile $\mathcal{O}_{\omega,0}(\boldsymbol{\rho}, z_0)$ and propagation constant $\beta_\omega = n_f(\omega)\omega/c$ like in a single mode fiber of effective refractive index n' [51] will not change the description:

$$\mathcal{O}_{\omega,j=0}(\boldsymbol{\rho}, z \geq z_0) = \mathcal{O}_{\omega,0}(\boldsymbol{\rho}, z_0)e^{i\beta_\omega(z-z_0)} \quad (\text{B5})$$

In a quantization volume $\mathcal{V} = \mathcal{S} \times \mathcal{L}$, a field in the mode $\mathcal{O}_{\omega,j}(\mathbf{r})$ will be said to be in the following quantum state :

$$|\mathcal{O}_{\omega,j}\rangle = \frac{1}{\sqrt{\mathcal{L}}} \int d^3\mathbf{r} \mathcal{O}_{\omega,j}(\mathbf{r})|1_{\mathbf{r}}\rangle \quad (\text{B6})$$

so that the states are normalized : $\langle \mathcal{O}_{\omega,j} | \mathcal{O}_{\omega,j'} \rangle = \delta_{jj'}$. Functions $\mathcal{O}_{\omega,j}(\mathbf{r})$ are only transversally normalized : $\int d^2\rho \mathcal{O}_{\omega,j'}^*(\boldsymbol{\rho}, z) \mathcal{O}_{\omega,j}(\boldsymbol{\rho}, z) = \delta_{jj'}$ and $\int_{\mathcal{V}} d^3\mathbf{r} \mathcal{O}_{\omega,j'}^*(\mathbf{r}) \mathcal{O}_{\omega,j}(\mathbf{r}) = \mathcal{L} \delta_{jj'}$.

b. Calculation of the transmitted field component

In a quantization volume containing a crystal before $z = z_0$ and a spatial filter at z_0 , a one-photon field in mode ℓ is in the state :

$$\begin{aligned} |1_\ell\rangle &= \int d^3\mathbf{r} f(\mathbf{r})|1_{\mathbf{r}}\rangle \\ &= \int d^3\mathbf{r} \left(\Theta(z_0 - z) \frac{e^{i\mathbf{k}_\ell \cdot \mathbf{r}}}{\sqrt{\mathcal{V}}} \right. \\ &\quad \left. + \Theta(z - z_0) \sum_j g_j(\ell) \frac{\mathcal{O}_{\omega_\ell,j}(\mathbf{r})}{\sqrt{\mathcal{L}}} \right) |1_{\mathbf{r}}\rangle \end{aligned} \quad (\text{B7})$$

$$+ \Theta(z - z_0) \sum_j g_j(\ell) \frac{\mathcal{O}_{\omega_\ell,j}(\mathbf{r})}{\sqrt{\mathcal{L}}} |1_{\mathbf{r}}\rangle \quad (\text{B8})$$

where $\Theta(z)$ is Heaviside's function and $g_j(\ell)$ are determined by the boundary conditions at $z = z_0$:

$$\sum_j g_j(\ell) \frac{\mathcal{O}_{\omega_\ell,j}(\boldsymbol{\rho}, z_0)}{\sqrt{\mathcal{L}}} = \frac{e^{i\boldsymbol{\kappa}'_\ell \cdot \boldsymbol{\rho}} e^{ik'_{z,\ell} z_0}}{\sqrt{\mathcal{V}}} \quad (\text{B9})$$

Remark that the wavevector takes into account the change of medium according to Snell-Descartes' law of refraction :

$$\frac{\boldsymbol{\kappa}'}{\kappa} = \frac{|\mathbf{k}'| \sin \theta'}{|\mathbf{k}| \sin \theta} = 1 \quad \frac{k'_z}{k_z} = \frac{|\mathbf{k}'| \cos \theta'}{|\mathbf{k}| \cos \theta} \approx \frac{n'}{n} \quad (\text{B10a})$$

where n' is the refractive index of the medium in which $\mathcal{O}_{\omega_\ell,j}(\mathbf{r})$ describes the spatial mode and n the refractive index in the crystal.

Using the orthonormality of functions $\{\mathcal{O}_{\omega,j}(\mathbf{r})\}$, one gets :

$$\begin{aligned} g_j(\ell) &= \int d^2\rho \mathcal{O}_{\omega_\ell,j}^*(\boldsymbol{\rho}, z_0) \frac{e^{i\boldsymbol{\kappa}'_\ell \cdot \boldsymbol{\rho}} e^{ik'_{z,\ell} z_0}}{\sqrt{\mathcal{V}}} \sqrt{\mathcal{L}} \\ &= \frac{1}{\sqrt{\mathcal{S}}} e^{ik'_{z,\ell} z_0} \check{\mathcal{O}}_{\omega_\ell,j}^*(\boldsymbol{\kappa}_\ell, z_0) \end{aligned} \quad (\text{B11})$$

where $\check{\mathcal{O}}_{\omega_\ell,j}(\boldsymbol{\kappa}, z_0)$ is the Fourier transform of $\mathcal{O}_{\omega_\ell,j}(\boldsymbol{\rho}, z_0)$ and * designates a complex conjugate.

Starting from an initial state $|\Psi(t_0)\rangle = \sum_\ell \mu_\ell |1_\ell\rangle$ localized at $z < z_0$, the state becomes for $z > z_0$:

$$|\Psi(t_1)\rangle = \sum_j \sum_\ell \mu_\ell e^{ik'_{z,\ell} z_0} \frac{1}{\sqrt{\mathcal{S}}} \check{\mathcal{O}}_{\omega_\ell,j}^*(\boldsymbol{\kappa}_\ell, z_0) |\mathcal{O}_{\omega_\ell,j}\rangle \quad (\text{B12})$$

Ignoring components of the state which are not within the mode $|\mathcal{O}_{\omega_\ell,0}\rangle$ transmitted by the filter, the transmitted one-photon state becomes :

$$\begin{aligned} |\Psi(t_1)\rangle &= \sum_\ell \mu_\ell e^{ik'_{z,\ell} z_0} \frac{1}{\sqrt{\mathcal{S}}} \check{\mathcal{O}}_{\omega_\ell,0}^*(\boldsymbol{\kappa}_\ell, z_0) |\mathcal{O}_{\omega_\ell,0}\rangle \\ &\quad + \text{ignored zero-photon states} \end{aligned} \quad (\text{B13})$$

Note that if one of the functions $\{\mathcal{O}_{\omega,j}(\mathbf{r})\}$ describes the spatial eigenmode of any other filter (e.g. a rectangular waveguide), the result is still valid.

As for spectral filtering, extrapolation to two-photon states is straightforward.

[1] W. Tittel and G. Weihs, *Quantum Information and Computation* **1**, 3 (2001).
[2] S. Gröblacher, T. Paterek, R. Kaltenbaek, *et al.*, *Nature* **446**, 871 (2007).
[3] N. Gisin and R. Thew, *Nature Photonics* **1**, 165 (2007), 10.1038/nphoton.2007.22.
[4] N. Gisin and R. T. Thew, *Electronics Letters* **46**, 965 (2010).
[5] A. K. Ekert, *Phys. Rev. Lett.* **67**, 661 (1991).

[6] J. H. Shapiro, *New Journal of Physics* **4**, 47 (2002).
[7] C. Simon, H. de Riedmatten, M. Afzelius, N. Sangouard, H. Zbinden, and N. Gisin, *Physical Review Letters* **98**, 190503 (2007).
[8] F. Wong, J. Shapiro, and T. Kim, *Laser Physics* **16**, 1517 (2006).
[9] P. G. Kwiat, K. Mattle, H. Weinfurter, A. Zeilinger, A. V. Sergienko, and Y. Shih, *Phys. Rev. Lett.* **75**, 4337 (1995).

- [10] T. G. Noh, H. Kim, T. Zyung, and J. Kim, *Appl. Phys. Lett.* **90**, 011116 (2007).
- [11] J. Altepeter, E. Jeffrey, and P. Kwiat, *Opt. Express* **13**, 8951 (2005).
- [12] B. Shi and A. Tomita, *J. Opt. Soc. Am. B* **21**, 2081 (2004).
- [13] H. Guillet de Chatellus, A. Sergienko, B. Saleh, M. Teich, and G. Di Giuseppe, *Opt. Express* **14**, 10060 (2006).
- [14] M. Fiorentino, C. Kuklewicz, and F. Wong, *Opt. Express* **13**, 127 (2005).
- [15] A. Fedrizzi, T. Herbst, A. Poppe, T. Jennewein, and A. Zeilinger, *Opt. Express* **15**, 15377 (2007).
- [16] O. Kuzucu and F. N. C. Wong, *Phys. Rev. A* **77**, 032314 (2008).
- [17] S. Virally, S. Lacroix, and N. Godbout, *Phys. Rev. A* **81**, 013808 (2010).
- [18] J. L. Smirr, R. Frey, E. Diamanti, R. Alléaume, and I. Zaquine, *J. Opt. Soc. Am. B* **28**, 832 (2011).
- [19] A. Lvovsky, B. Sanders, and W. Tittel, *Nature Photonics* **3**, 706 (2009).
- [20] Simon, C., Afzelius, M., Appel, J., Boyer de la Giroday, A., Dewhurst, S. J., Gisin, N., Hu, C. Y., Jeletzko, F., Kröll, S., Müller, J. H., Nunn, J., Polzik, E. S., Rarity, J. G., De Riedmatten, H., Rosenfeld, W., Shields, A. J., Sköld, N., Stevenson, R. M., Thew, R., Walmsley, I. A., Weber, M. C., Weinfurter, H., Wrachtrup, J., and Young, R. J., *Eur. Phys. J. D* **58**, 1 (2010).
- [21] T. Chanelière, J. Ruggiero, M. Bonarota, M. Afzelius, and J.-L. L. Gouët, *New Journal of Physics* **12**, 023025 (2010).
- [22] E. Saglamyurek, N. Sinclair, J. Jin, J. Slater, D. Oblak, F. Bussièeres, M. George, R. Ricken, W. Sohler, and W. Tittel, *Nature* **469**, 512 (2011).
- [23] W. H. Louisell, A. Yariv, and A. E. Siegman, *Phys. Rev.* **124**, 1646 (1961).
- [24] C. K. Hong and L. Mandel, *Phys. Rev. A* **31**, 2409 (1985).
- [25] R. Ghosh and L. Mandel, *Phys. Rev. Lett.* **59**, 1903 (1987).
- [26] L. Mandel, *Rev. Mod. Phys.* **71**, S274 (1999).
- [27] M. H. Rubin, D. N. Klyshko, Y. H. Shih, and A. V. Sergienko, *Phys. Rev. A* **50**, 5122 (1994).
- [28] T. E. Keller and M. H. Rubin, *Phys. Rev. A* **56**, 1534 (1997).
- [29] T. B. Pittman, D. V. Strekalov, D. N. Klyshko, M. H. Rubin, A. V. Sergienko, and Y. H. Shih, *Phys. Rev. A* **53**, 2804 (1996).
- [30] A. Joobeur, B. E. A. Saleh, and M. C. Teich, *Phys. Rev. A* **50**, 3349 (1994).
- [31] C. Kurtsiefer, M. Oberparleiter, and H. Weinfurter, *Phys. Rev. A* **64**, 023802 (2001).
- [32] F. A. Bovino, P. Varisco, A. M. Colla, G. Castagnoli, G. D. Giuseppe, and A. V. Sergienko, *Optics Communications* **227**, 343 (2003).
- [33] S. Castelletto, I. P. Degiovanni, A. Migdall, and M. Ware, *New Journal of Physics* **6**, 87 (2004).
- [34] S. Castelletto, I. Degiovanni, G. Furno, V. Schettini, A. Migdall, and M. Ware, *Instrumentation and Measurement, IEEE Transactions on* **54**, 890 (2005).
- [35] D. Ljunggren and M. Tengner, *Phys. Rev. A* **72**, 062301 (2005).
- [36] A. Ling, J. Chen, J. Fan, and A. Migdall, *Opt. Express* **17**, 21302 (2009).
- [37] M. W. Mitchell, *Phys. Rev. A* **79**, 043835 (2009).
- [38] R. S. Bennink, *Phys. Rev. A* **81**, 053805 (2010).
- [39] R. Boyd, *Nonlinear optics* (Academic Press, 2008).
- [40] A. Yariv, *Quantum electronics* (Wiley, 1989).
- [41] M. Fiorentino, G. Messin, C. E. Kuklewicz, F. N. C. Wong, and J. H. Shapiro, *Phys. Rev. A* **69**, 041801 (2004).
- [42] M. Hentschel, H. Hübel, A. Poppe, and A. Zeilinger, *Opt. Express* **17**, 23153 (2009).
- [43] J. Garrison and R. Chiao, *Quantum optics* (Oxford University Press, 2008).
- [44] J. Shapiro, *Selected Topics in Quantum Electronics, IEEE Journal of* **15**, 1547 (2009).
- [45] The natural phase matching bandwidth has no influence on the results that follow if it is much larger than the pump linewidth.
- [46] J. Berntsen, T. O. Espelid, and A. Genz, *ACM Trans. Math. Softw.* **17**, 437 (1991).
- [47] G. D. Boyd and D. A. Kleinman, *J. Appl. Phys.* **39**, 3597 (1968).
- [48] J. L. Smirr, S. Guilbaud, J. Ghalbouni, R. Frey, E. Diamanti, R. Alléaume, and I. Zaquine, *Opt. Express* **19**, 616 (2011).
- [49] A. Ling, A. Lamas-Linares, and C. Kurtsiefer, *Phys. Rev. A* **77**, 043834 (2008).
- [50] L. Mandel, *Phys. Rev.* **144**, 1071 (1966).
- [51] A. Ghatak and K. Thyagarajan, *Introduction to fiber optics* (Cambridge University Press, 1998).